

AD-A119 468

SCIENCE APPLICATIONS INC MCLEAN VA  
RADIATION FROM HIGH TEMPERATURE PLASMAS. PHASE II. (U)  
AUG 82 C AGRITELLIS

F/G 20/9

N00014-81-C-2398

UNCLASSIFIED

SAI-83-883-WA

NL

1-1  
31-3-82



END  
DATE  
FILMED  
10-82  
DTIC



12

RADIATION FROM HIGH TEMPERATURE PLASMAS -

PHASE II

FINAL REPORT

SAI-83-883-WA

DTIC

SEP 22 1982

H



ATLANTA • ANN ARBOR • BOSTON • CHICAGO • CLEVELAND • DENVER • HUNTSVILLE • LA JOLLA  
LITTLE ROCK • LOS ANGELES • SAN FRANCISCO • SANTA BARBARA • TUCSON • WASHINGTON

DISTRIBUTION STATEMENT A

Approved for public release;  
Distribution Unlimited

**RADIATION FROM HIGH TEMPERATURE PLASMAS -  
PHASE II**

**FINAL REPORT**

**SAI-83-883-WA**

**Submitted to:**

**Plasma Radiation Branch  
Plasma Physics Division  
Naval Research Laboratory  
Washington, D.C. 20375**

**Prepared Under:**

**Contract No. N00014-81-C-2398  
SAI Project No. 1-157-18-438-00**

**Prepared by:**

**Christopher Agritellis**

**SCIENCE APPLICATIONS, INC.**

**1710 Goodridge Drive, McLean, VA 22102  
(703) 734-5840**

SECURITY CLASSIFICATION OF THIS PAGE (When Data Entered)

| REPORT DOCUMENTATION PAGE   |   | READ INSTRUCTIONS<br>BEFORE COMPLETING FORM                                 |
|---|---|---|
| 1. REPORT NUMBER  | 2. GOVT ACCESSION NO.<br><b>AD A119 468</b> | 3. RECIPIENT'S CATALOG NUMBER   |
| 4. TITLE (and Subtitle)<br><br>Radiation from High Temperature Plasmas<br>Phase II  |   | 5. TYPE OF REPORT & PERIOD COVERED<br>Final Report<br>15 Jul 81 - 14 Jul 82 |
| 7. AUTHOR(s)<br><br>Christopher Agritellis  |   | 6. PERFORMING ORG. REPORT NUMBER  |
| 9. PERFORMING ORGANIZATION NAME AND ADDRESS<br>Science Applications, Inc.<br>1710 Goodridge Dr.<br>McLean, VA. 22102  |   | 8. CONTRACT OR GRANT NUMBER(s)<br><br>N00014-81-C-2398                      |
| 11. CONTROLLING OFFICE NAME AND ADDRESS<br>Naval Research Laboratory<br>4555 Overlook Avenue, S.W.<br>Washington, D.C. 20375  |   | 10. PROGRAM ELEMENT, PROJECT, TASK<br>AREA & WORK UNIT NUMBERS              |
| 14. MONITORING AGENCY NAME & ADDRESS (if different from Controlling Office)   |   | 12. REPORT DATE<br>August 1982  |
|   |   | 13. NUMBER OF PAGES   |
|   |   | 15. SECURITY CLASS. (of this report)<br><br>Unclassified                    |
|   |   | 15a. DECLASSIFICATION/DOWNGRADING<br>SCHEDULE                               |
| 16. DISTRIBUTION STATEMENT (of this Report)   |   |   |
| <div style="border: 1px solid black; padding: 5px; text-align: center;"> <b>DISTRIBUTION STATEMENT A</b><br/>           Approved for public release;<br/>           Distribution Unlimited         </div>   |   |   |
| 17. DISTRIBUTION STATEMENT (of the abstract entered in Block 20, if different from Report)  |   |   |
| 18. SUPPLEMENTARY NOTES   |   |   |
| 19. KEY WORDS (Continue on reverse side if necessary and identify by block number)<br><br>Plasma radiation, radiation hydrodynamics, atomic physics,<br>imploding targets, nuclear weapons simulation, x-ray spectra.   |   |   |
| 20. ABSTRACT (Continue on reverse side if necessary and identify by block number)<br><br>A large number of atomic physics and magnetohydrodynamic<br>computer codes have been developed by members of the NRL<br>Plasma Radiation Branch of the Naval Research Laboratory over<br>several years. These codes involve the simulation of complex<br>physical processes in a variety of plasma radiation research<br>investigations. In this research effort, the structure of many<br>of these codes was analyzed to improve the numerical procedures |   |   |

DD FORM 1473  
1 JAN 73

EDITION OF 1 NOV 68 IS OBSOLETE  
S/N 0102-LF-014-6601

SECURITY CLASSIFICATION OF THIS PAGE (When Data Entered)

or to speed calculational time by code vectorization. In addition, graphic techniques were developed to improve the display of the results, which is important both to detect coding errors and to elucidate physical mechanisms. In this report, we describe the codes that were improved and present examples of the graphical displays now available for analysis of the calculational results.

|                    |                                     |
|--------------------|-------------------------------------|
| Accession For      |                                     |
| NTIS               | <input checked="" type="checkbox"/> |
| DTIC               | <input type="checkbox"/>            |
| Unannounced        | <input type="checkbox"/>            |
| Justification      | <i>for</i>                          |
| By                 |                                     |
| Distribution       |                                     |
| Availability Codes |                                     |
| Dist               | Avail and/or Special                |
| <b>A</b>           |                                     |



## TABLE OF CONTENTS

| <u>Section</u> |                                | <u>Page</u> |
|----------------|--------------------------------|-------------|
| I              | INTRODUCTION . . . . .         | 1           |
| II             | ATOMIC PHYSICS CODES . . . . . | 1           |
| III            | MHD CODES . . . . .            | 3           |
|                | ACKNOWLEDGEMENTS . . . . .     | 10          |

## I. INTRODUCTION

The primary objectives of this research effort were to provide numerical and computational support in terms of code conversions, code improvement, and the development of graphic techniques and codes as well as provide analytical support in a number of radiation/matter interaction investigations. Each of these items are individually discussed below starting with the various codes and their functions. Also a short description of each code is presented for the purposes of documentation.

The Plasma Radiation Branch of NRL is involved in a number of highly diverse activities ranging from studies in basic atomic physics and collision processes to radiation hydrodynamics of imploding targets and nuclear weapons environment simulations. In order to describe the physics of such a variety of disciplines a number of computer simulations and codes must be constructed and developed. Most of these codes are generated internally in the Branch although some of them are transferred from other research institutes and different computer facilities. It is inevitable that some of these codes are unvectorizable due to their logical structure and numerical techniques employed.

When a computer program is vectorized, the use of the ASC, which is a vector machine, is recommended. In this case the ASC runs are at least a factor of 3 more cost effective than identical runs on similar non vector machines. The VAX, which is a non vector machine, is superior to the ASC only when the codes are completely unvectorized but again this superiority is impaired by the complete absence of batch program facilities and fast printer availability.

## II. ATOMIC PHYSICS CODES

A set of atomic physics codes from the NRL Plasma Radiation Branch was converted from ASC to VAX. The distorted wave scattering code "DIRECT", the Dipole Transition Potential TRANP using known wave functions of inner electrons, and the program "SPINFL" which calculates collision strength,  $\Omega$ , for any transition between levels A, B of an atom with 2 electrons outside closed shells have been improved and converted to VAX.

The main objective of this activity is to generate a radial wave function  $P_{n,l}$  by solving the equation:

$$\left[ \frac{d^2}{dr^2} - \frac{l(l+1)}{r^2} - 2V(r) + 2E \right] P_{nl}(r) = 0, \quad (1)$$

where  $E$  is the energy of the atom level considered, and the potential energy  $V(r)$  may be given in two different forms:

(a) Screened potential

$$V(r) = -\frac{Z_n}{r} + \frac{1}{r} \int_0^r \sum_i q_i P_i^2 dx + \int_r^\infty \sum_i q_i \alpha^{-1} P_i^2 dx$$

$$- \frac{\alpha}{2r} \left[ \frac{81}{4\pi^2} r \sum_i q_i P_i^2 \right]^{1/3} - \frac{\alpha_d}{2r^4} \left[ 1 - \exp(-r/r_1)^6 \right] \quad (2)$$

- $Z_n$  = charge of the nucleus,
- $q_i$  = number of equivalent core electrons given by the wave function  $P_i$   
 $(\sum_i q_i = \text{total number of core electrons}),$
- $\alpha$  = adjustable constant,
- $\alpha_d$  = dipole polarizability of the core,
- $r_1$  = parameter for the polarization potential.

The first three terms on the right-hand side of (2) represent the potential due to the nuclear charge and the screening of core electrons (spherically averaged). The fourth term is the "exchange-correlation potential" similar to the definition given by Slater (but not identical to it), and the last term is the polarization potential.

This form of  $V(r)$  is convenient if  $P_i$  of core electrons are known. Parameters  $\alpha_d$  and  $r_1$  for the polarization potential are known only rarely and may be omitted.

(b) Analytical potential

$$V(r) = -\frac{1}{r} Z + (Z_n - Z) \exp(-\alpha Z r) \quad (3)$$

where

$Z_n$  = charge of the nucleus,

$Z$  = asymptotic charge of the atomic core ( $Z = Z_n$  - number of core electrons),

$\alpha$  = adjustable constant.

The value of  $\alpha$  is chosen to give correct asymptotic behavior of  $P_n$ . This form of  $V(r)$  is convenient if wave functions or core electrons are not known.

### III. MHD CODES

Numerical and computational support and conversion to VAX is provided for the cylindrical core/corona mode "SPLAT" and the Hartree-Fock atomic physics code RCN from LASL which calculates atomic structure parameters. The SPLAT code is a time-dependent self-similar implosion code with 1D radial fluid grid which is moved in a Lagrangian sense and enables one to track the local neutral plasma position, velocity, and acceleration fields. The ion density is the fundamental fluid quantity which is evolved and the ion fluid is heated through all appropriate physical processes and cooled through expansion and by radiation. The electron heating takes place by compression, viscous, ohmic heating and core/corona heat exchange and radiative losses. The RCN code from LASL is used for the self-consistent-field calculation of atomic radial wave-functions and radial integrals involved in the calculation of atomic energy levels and spectra. The calculation is of radial wavefunctions of a spherically-symmetrized atom, corresponding to the center of gravity energy of an electron. From these radial wavefunctions the coulomb integrals and the spin-orbit integrals are computed.

When the radial component  $R_{n,l}$  of the eigenfunction  $\psi = \Phi_m \Theta_{m,l} R_{n,l}$  is multiplied by  $R_{n,l}^*$  then the product  $R_{n,l} R_{n,l}^*$  gives the probability-density distribution  $\psi\psi^*$  as a function of the nuclear-electron distance  $r$ .

The radial equation

$$\frac{1}{r^2} \frac{\partial}{\partial r} \left( r^2 \frac{\partial R}{\partial r} \right) - \frac{l(l+1)}{r^2} R + \frac{8\pi^2 \mu}{h^2} (W-V) R = 0$$

$$\text{where } W = \pm \frac{2\pi^2 \mu e^4 Z^2}{n^2 h^2}, \quad V = \frac{e^2 Z}{r}, \quad r = \frac{nh^2}{8\pi^2 \mu e^2 Z} x$$

has a solution

$$R_{n,l} = \left( \frac{4(n-l-1)! Z^3}{[(n+l)!] 3^4 n^4 \alpha_1^3} \right)^{\frac{1}{2}} \left( \frac{2Zr}{n\alpha_1} \right)^l \cdot \exp\left(-\frac{Zr}{n\alpha_1}\right) \cdot L_{n+l}^{2l+1} \left( \frac{2Zr}{n\alpha_1} \right)$$

and the expression  $L_{n+l}^{2l+1} \left( \frac{2Zr}{n\alpha_1} \right)$  are derivatives of the Laquerre polynomials.

The function  $D = 4\pi r^2 (R_{n,l})^2$  is the probability-density function and represents the probability of finding the electron with quantum numbers  $n, l$  between two spheres of radius  $r$  and  $r+dr$ . Modeling the hydrogenic electron we can plot the radial function  $R_{n,l}$ ,  $(R_{n,l})^2$  and the probability-density function  $D$  as a function of the electron distance  $r$  for various atomic numbers and  $n$  and  $l$ .

Special codes and models were developed in order to obtain the radial function  $R_{n,l}$ , the probability-density factor, and the density distribution  $D$  of a wave function of an electron. Examples of these graphs are given below (Figures 1-9). In some of these graphs charge distribution of non-hydrogenic cases are compared with wave functions of more complicated programs.

In the Bohr-Sommerfeld calculations of the elliptic orbits an electron with total quantum number  $n$  and azimuthal quantum number  $k$  has semimajor axis  $a$  and semiminor axis  $b$  given by:

$$a = a_1 \frac{n^2}{Z}, \quad b = a_1 \frac{nk}{Z}$$

where  $a_1$  is the first Bohr orbit radius. For  $k = n$  we have circular orbits and for  $k=1,2,\dots,(n-1)$  elliptic orbits. The  $k=0$  straight line orbit is excluded. The discreteness of the energy states in the Bohr-Sommerfeld case is introduced quite artificially. On the contrary in the case of the solution of the Schrodinger equation the discreteness appears quite naturally as the solution of the Schrodinger equation.

In Figures 1 and 2 the electron charge distribution : of Cowan's LASL calculations for Al XI 2s and 1s electrons is compared with our (dotted line) calculation. In Figure 3 our calculations are compared with TRANSP (Milan) calculations for the Al XI 3d electron. The units of length in all plots are in first Bohr circular orbit radius.

In Figures 4, 5, and 6 the Radial factor  $R_{n,l}$ , the probability density function  $D = 4\pi^2 (R_{n,l})^2$ , and the Radial factor  $(R_{n,l})^2$  are plotted respectively in 3-D for the hydrogenic electron  $n=8$  and  $l=3$ . The number of peaks (or rings) in the  $(R_{n,l})^2$  and  $D = 4\pi^2 (R_{n,l})^2$  case is equal to the difference  $(n-l)$ . For the  $n=8$ ,  $l=3$  case the number of rings is five and the plots show the radial distribution of the electron around the nucleus with five maxima. Since we consider only the radial component  $R_{n,l}$  there is a rotation symmetry for the azimuthal angle  $\theta$  and the angle  $\phi$ .

In Figure 7 we see a 3-D plot of the probability-density function for the hydrogenic electron 2s ( $n=2$ ,  $l=0$ ). In the cross section across the x axis we observe two maxima for the peaks since  $n-l=2$ . This cross section is reminiscent of Figure 1. There we had the charge distribution of a 2s electron in Al XI. There the peaks were at different distances from the center of the nucleus. Figure 8 shows the whole view of Figure 7 from a different position of the camera.

The solution of the differential equation

$$\frac{1}{\theta} \frac{1}{\sin \theta} \frac{\partial}{\partial \theta} \left( \sin \theta \frac{\partial \Theta}{\partial \theta} \right) - \frac{m^2}{\sin^2 \theta} + \ell(\ell+1) = 0$$

is the angular component  $\Theta_{m,\ell}$  of the eigenfunction  $\psi$

$$\Theta_{m,\ell} = \left( \frac{(2\ell+1)(\ell-m)!}{2(\ell+m)!} \right)^{\frac{1}{2}} \cdot \sin^m \theta \cdot P_{\ell}^m(\cos \theta)$$

where  $P_{\ell}^m(\cos \theta)$  is the associated Legendre polynomial. The product  $\Theta_{m,\ell} \cdot \sin \theta d\theta$  is the probability of finding the electron between  $\theta$  and  $\theta+d\theta$ .

The complete eigenfunction is

$$\psi_{m,\ell,n} = \phi_m \cdot \Theta_{m,\ell} \cdot R_{\ell,n}$$

and the probability-density factors (for symmetric  $\phi$ ) for the radial and angular components  $(\Theta_{m,\ell})^2$  and  $(R_{\ell,n})^2$  give the probability densities for finding the electron between two spheres of radius  $r$  and  $r+dr$  and azimuthal angle between  $\theta$  and  $\theta+d\theta$ .

Programs calculating the Legendre polynomials for the angular component of the wave function are developed. Using the radial and angular distribution the probability density of hydrogenic electrons of any combination of  $n$ ,  $\ell$ , and  $m$  can be plotted. A few examples are given in Figures 9 through 15.

The number  $N$  of the wings in the butterfly of the angular component  $\Theta_{\ell m}$  for an electron with quantum numbers  $\ell$  and  $m$  is given by:

$$N = 2 * (\ell - m + 1)$$

In Figures 10, 11, 12, and 13 we see how the angular distributions  $\Theta_{33}$ ,  $\Theta_{32}$ ,  $\Theta_{31}$ , and  $\Theta_{30}$  change the probability density of the hydrogenic

electron  $n=8$ ,  $l=3$  in the five rings of the radial distribution  $R_{83}$  of Figure 9. Figures 13, 14 and 15 show the radial and angular probability-density for different combinations of the quantum numbers  $n, l$ , and  $m$ .

The old SERDY program was restructured and improved. SERDY is a hydro-transport, radiation energy deposition, radiation transport and thermal conduction program. The physics in this spherical-equilibrium-radiation-dynamics program with respect to the hydrodynamic equations accounting for radiation energy pressure and radiant heat exchange was corrected so that an investigation of an argon seeded microballoon implosion could be possible. The results of this investigation were presented at the APS, Division of Plasma Physics Meeting, October 1981. The following are abstracts of two papers delivered at the APS, New York Meeting.

CRE Analysis of Argon Puff Gas K-Series Emission Spectra+.

K.G. WHITNEY, C. AGRITELLIS\*, AND J. DAVIS, Naval Research Laboratory. --In collisional-radiative equilibrium (CRE), the strength of argon puff gas spectral features, both relative and absolute, is a direct reflection of the distribution of strengths of collisional and radiative couplings within the plasma. A detailed atomic model of argon has been constructed containing extensive level structure in Ar XVI, XVII, and XVIII, Lyman and Balmer series line couplings in Ar XVII and Ar XVIII, eight of the dominant line couplings in Ar XVI, and Gaunt factor contributions to the continuum free-bound emission background. Using this model, we will describe the behavior of instrumentally broadened, optically thick argon K-shell emission spectra under the influence of temperature and density gradients and as a function of the degree of plasma compression and plasma mass.

+ This work was supported by DNA

\* Science Applications, Inc. McLean, Va.

Radiation Hydrodynamics of a Radiation Imploded Argon Microballoon+.

C. AGRITELLIS\*, K. G. WHITNEY and J. DAVIS, Naval Research Laboratory. --The radiation hydrodynamics of a radiation imploded argon microballoon is

investigated. The mode includes an absorption mechanism, non-LTE radiation physics, line and continuum radiation transfer, spectral line profile functions and hydrodynamics. The purpose of this investigation is to study the behavior of detailed K-shell emission spectra as a function of initial driver conditions. Detailed comparisons will be made between the continuum intensity spectral line intensity and widths, and continuum edge effects for several initial conditions.

+ Work supported by Defense Nuclear Agency

\* Science Applications, Inc. McLean, Va.

While X-ray spectra from imploded plasmas are often used to infer an average plasma temperature and density, these are necessarily uneconomical diagnostics since there is generally a considerable amount of space-time variability to plasma temperatures and densities during the compression and subsequent expansion stages. We have investigated the influence of temperature and density gradients, at an instant of time, on the structure of the collisional-radiative couplings within a compressing, spherical plasma and correlated these structures with the shape and intensity of the instantaneous emission spectrum. It is theoretically possible to accurately generate and analyze temporally and spectrally resolved broadband emission spectra from imploded plasmas that leave complicated temperature and density profiles. It is important to obtain absolute (spectrally resolved) calorimeter data, plasma size information, as well as film spectral data in order to make unambiguous theoretical interpretations of emission spectra from optically thick plasmas. The so-called small discrepancies that are seen in line ratios that are used to predict the temperature for imploded plasmas may be indicators that the plasma has no well defined temperature but rather large temperature and density gradients. For each of the argon emission features within the spectrum, we use the ratios of photo-excitation to electron collisional excitation as a measure of the structure of the collisional-radiative couplings within the plasma. These ratios, which vary throughout the plasma volume, are plotted in Figure 17 and 18 in the form of a histogram with plasma cells

represented along the y-axis and the lines and edges represented along the x-axis. Low frequency lines are characterized by high electron collisional excitation values while the high frequency lines and the edges have very high photo excitation performance.

Graphic programs and packages are created for diagnostic purposes and multi-color presentation of non-LTE radiation from argon seeded microballoon implosion using NRL/LASNEX and NRL hydrodynamics models. Color pictures were created corresponding to K-Shell X-Ray emission in the compression phase from an argon microballoon using the NRL/LASNEX radiation model. In Figures 19 and 20 the electron temperature and density gradients are shown in a compressed spherical plasma along with the shape and intensity of the instantaneous emission spectrum. Two color movies of the compression and a set of pictures of the full spectrum at different times provide a spectacular view of the whole event. A color movie for the NRL radiation case and a set of color pictures for both APS presented papers have already been delivered to NRL.

#### ACKNOWLEDGEMENTS

This work was supported under contract number N00014-81-C-2398 with the Plasma Radiation Branch of the Plasma Physics Division of the Naval Research Laboratory. We would like to thank members of this branch and, in particular, Dr. Jack Davis for many valuable discussions during the performance of the contract and in the preparation of the final report.

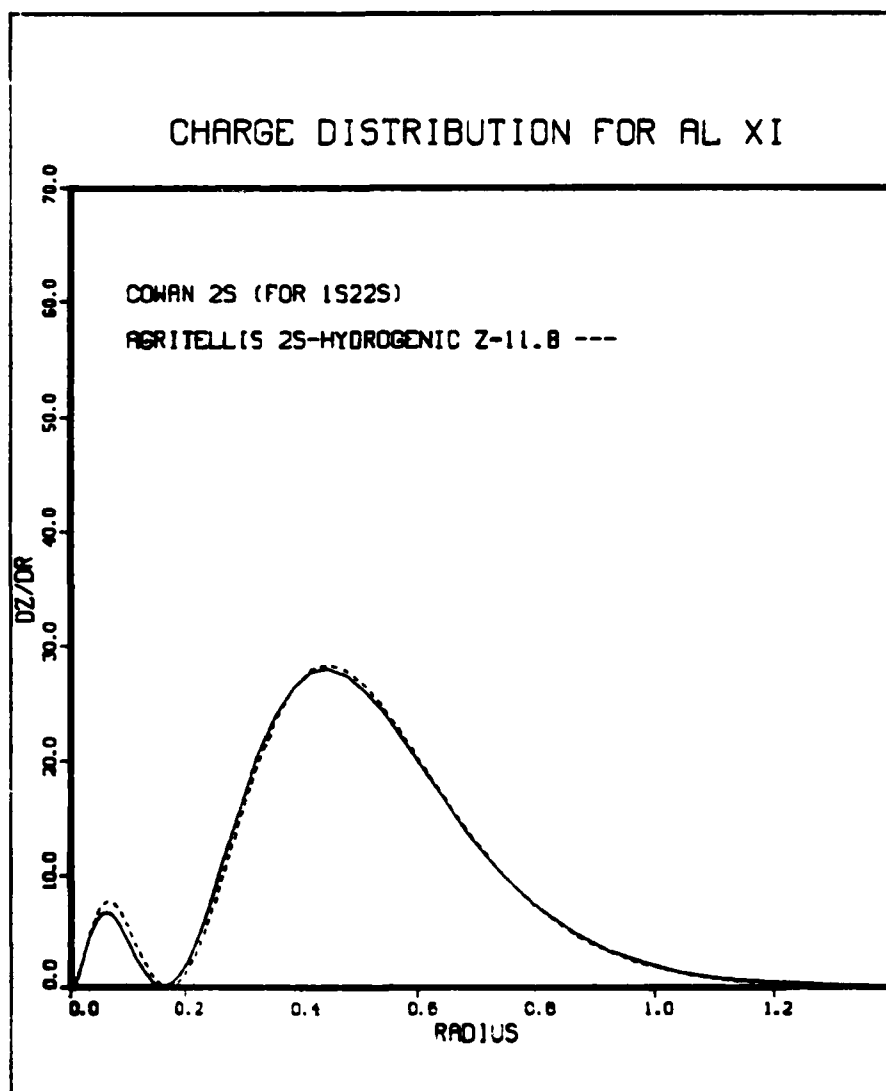


Fig. 1. Charge Distribution of a 2s electron in Al XI Compared with LASL (Cowan) Program

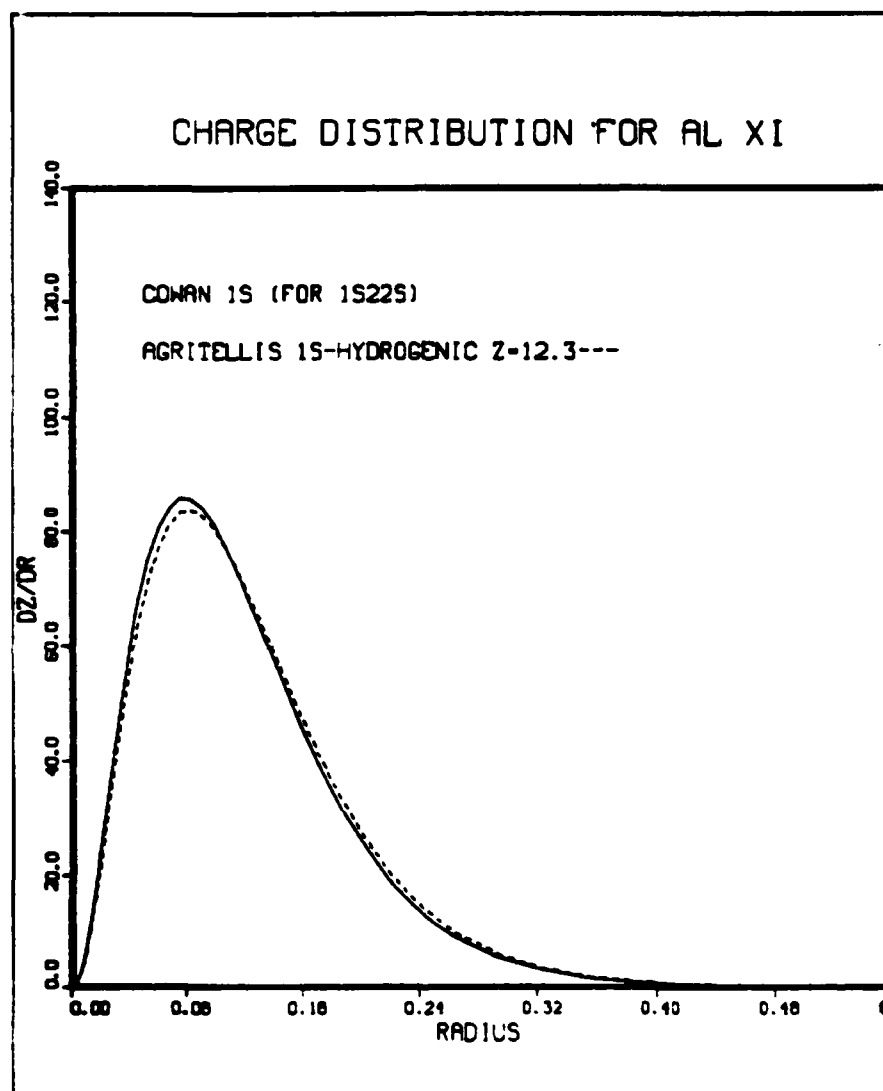


Fig. 2. Charge Distribution of a 1s electron in Al XI Compared with LASL (Cowan) Program

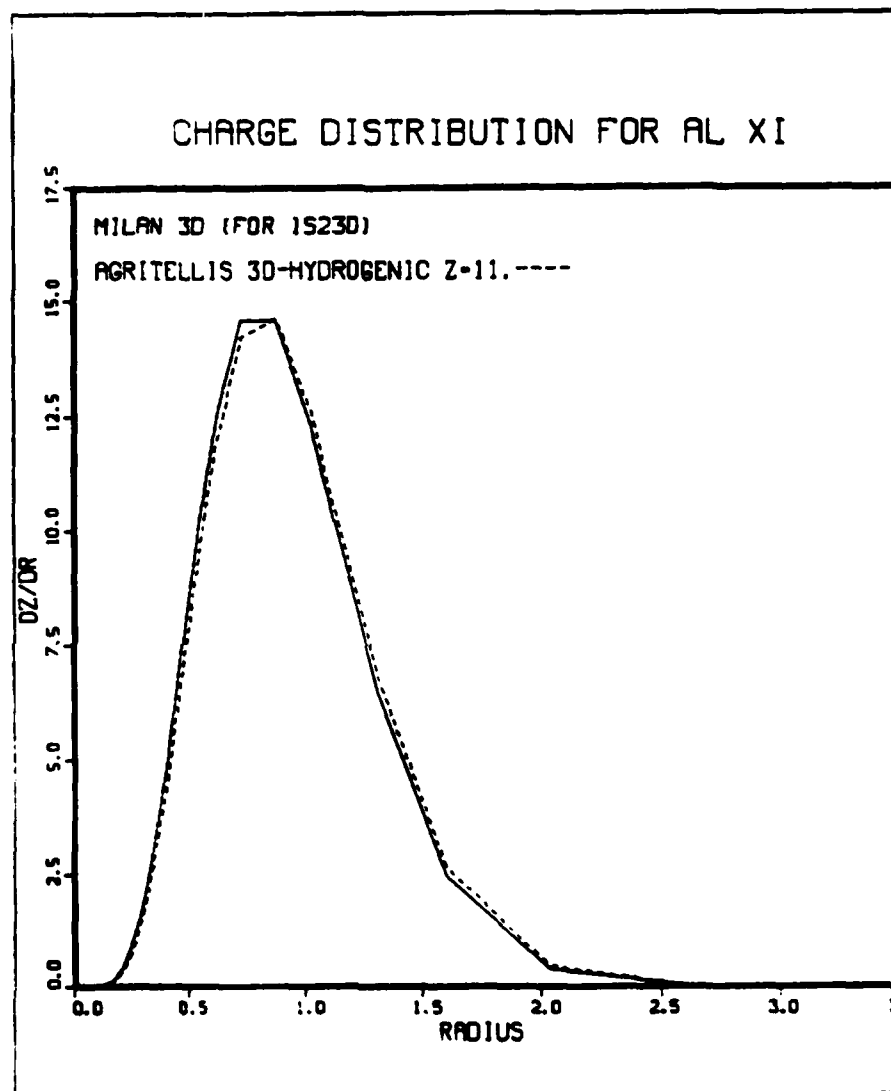


Fig. 3. Charge Distribution of a 3d electron in Al XI Compared with NRL-MILAN Program

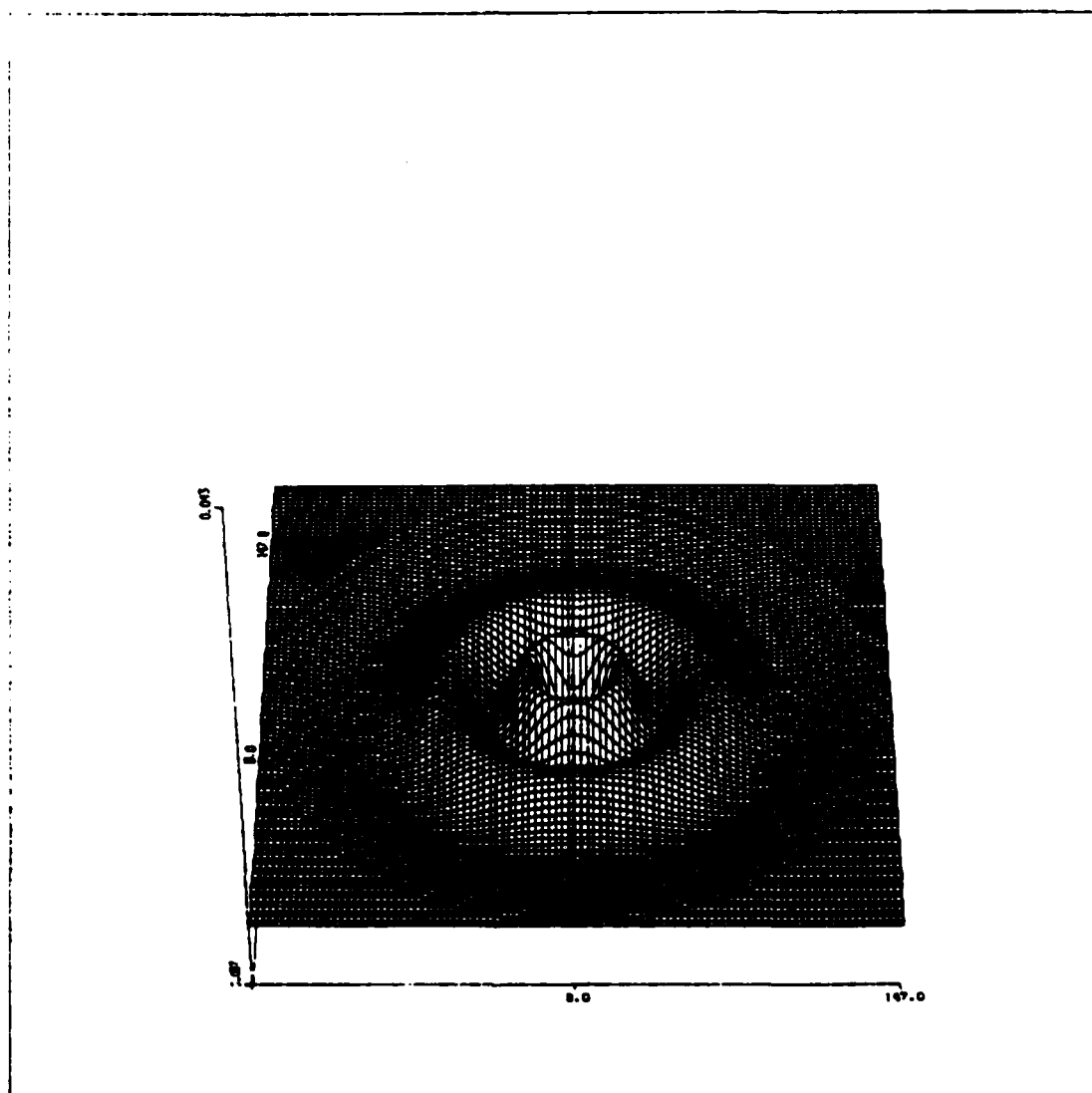


Fig. 4. Radial Factor  $R_{n,l}$  for Hydrogen  $n = 8$ ,  $l = 3$

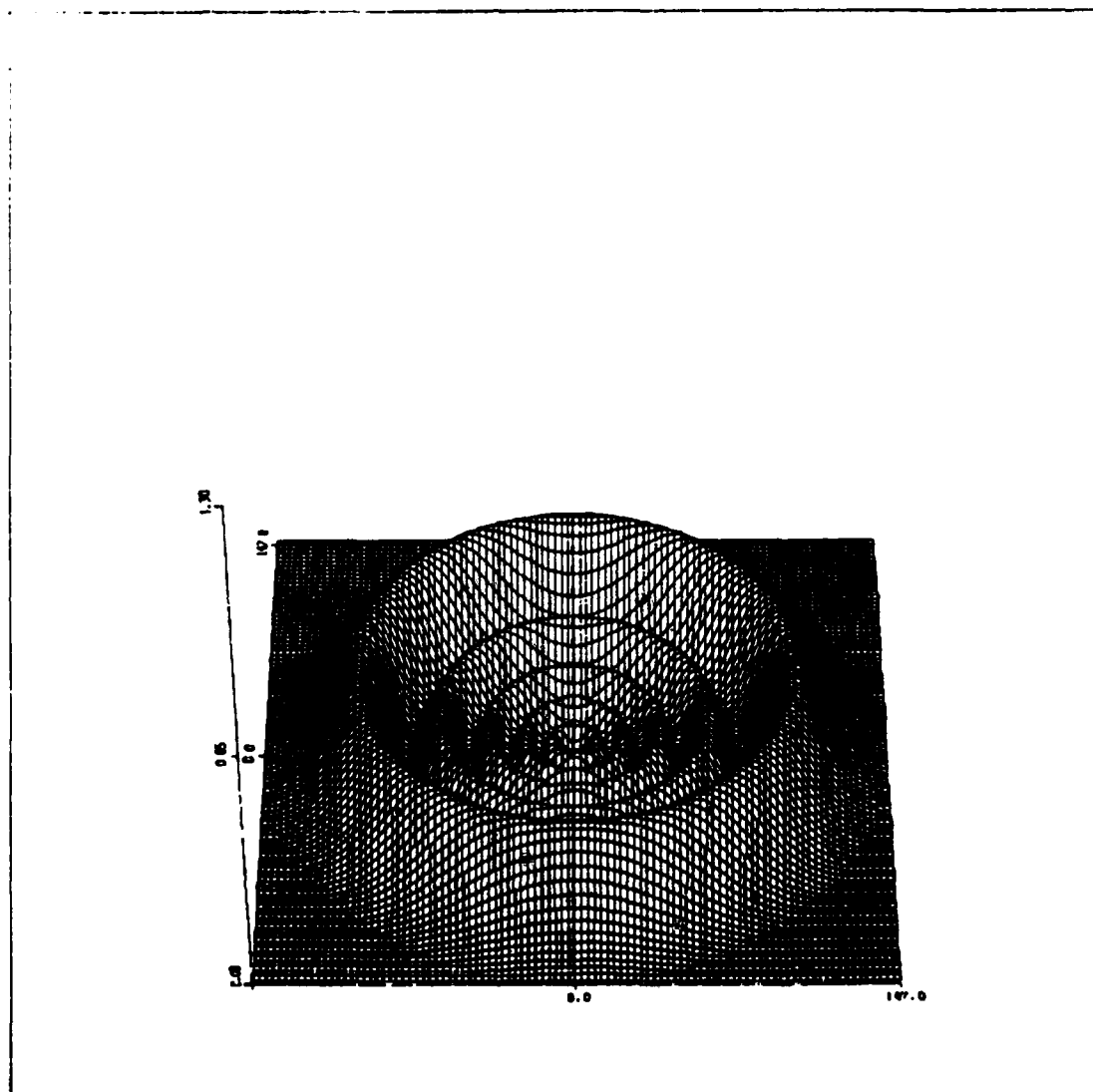


Fig. 5. Probability-Density Function for  $n = 8$ ,  $l = 3$

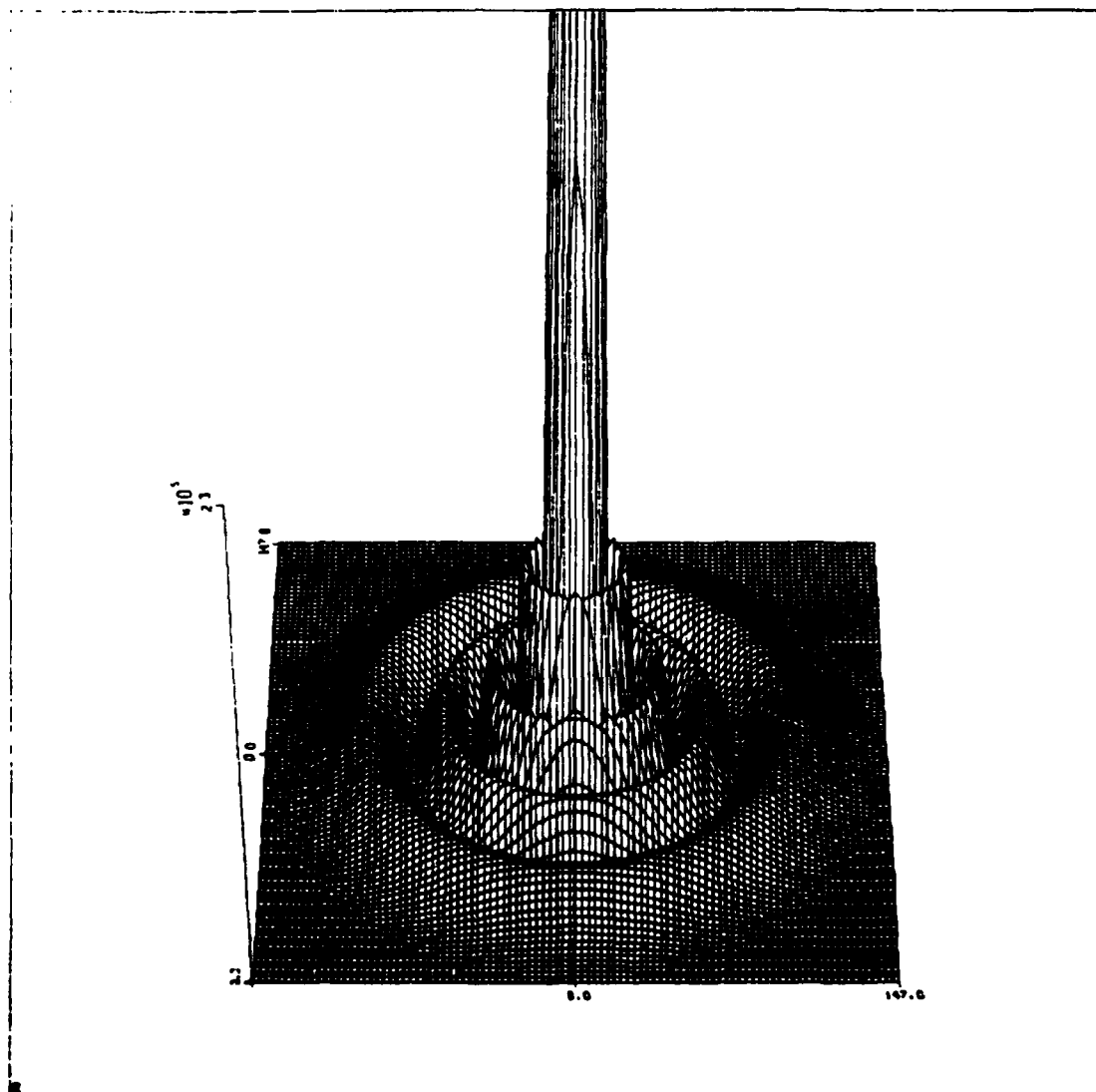


Fig. 6. Radial Factor  $(R_{n,l})^2$  for Hydrogen  $n = 8, l = 3$

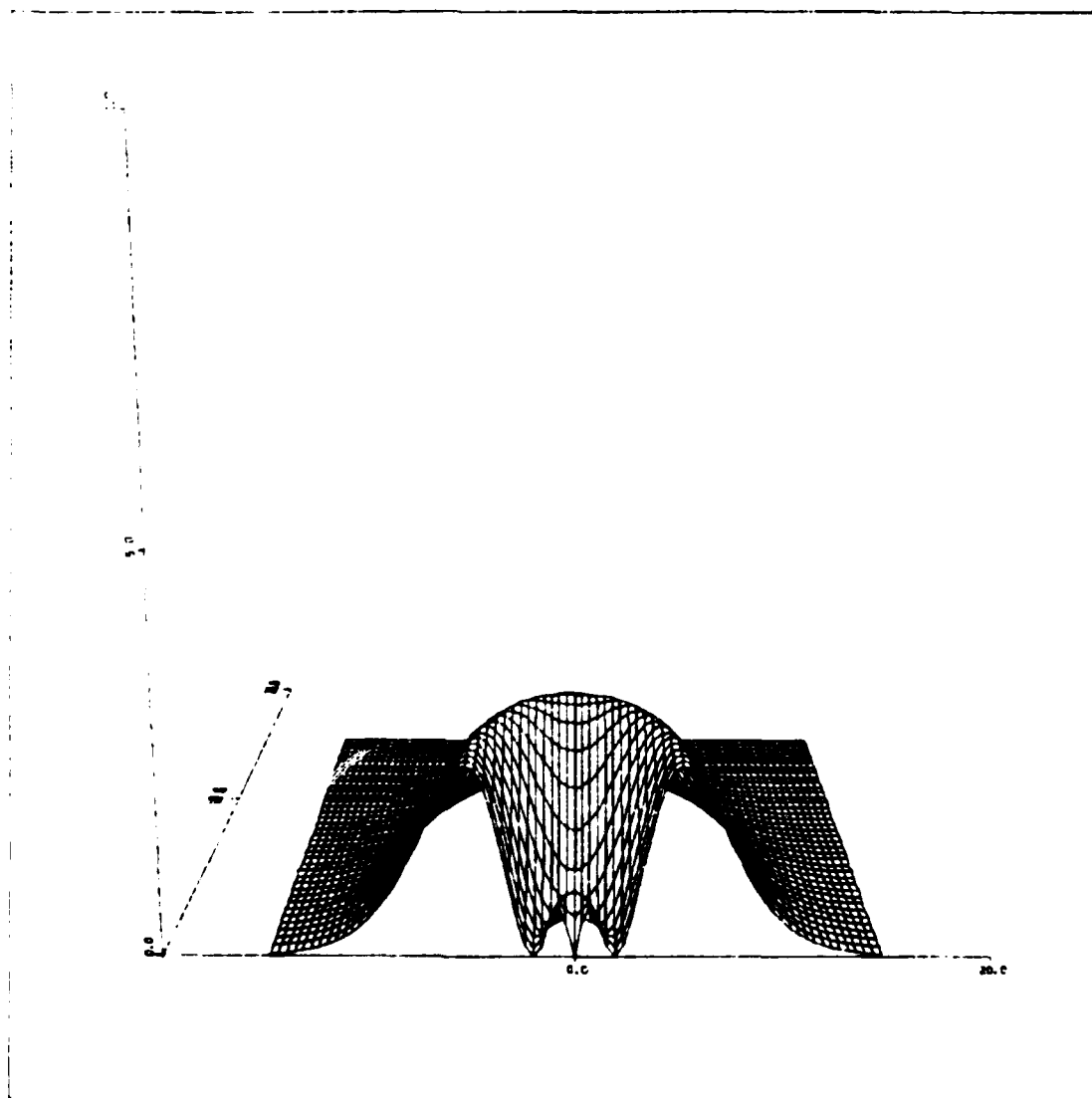


Fig. 7. Probability-Density Function  $D = 4\pi r^2 (R_{n,l})^2$  for a 2s Electron

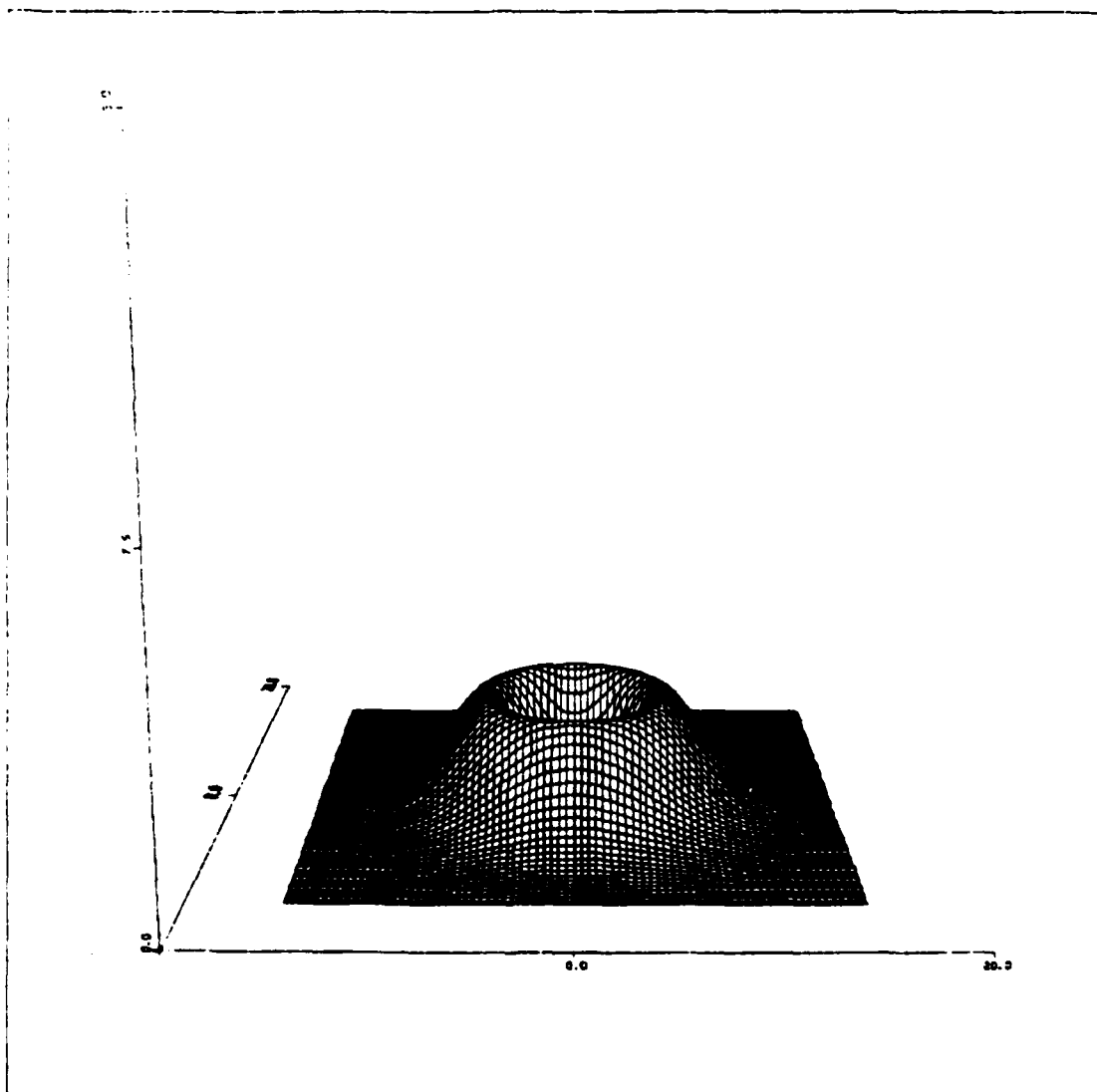


Fig. 8. Probability-Density Function  $D = 4\pi r^2 (R_{n,l})^2$  for a 2s Electron

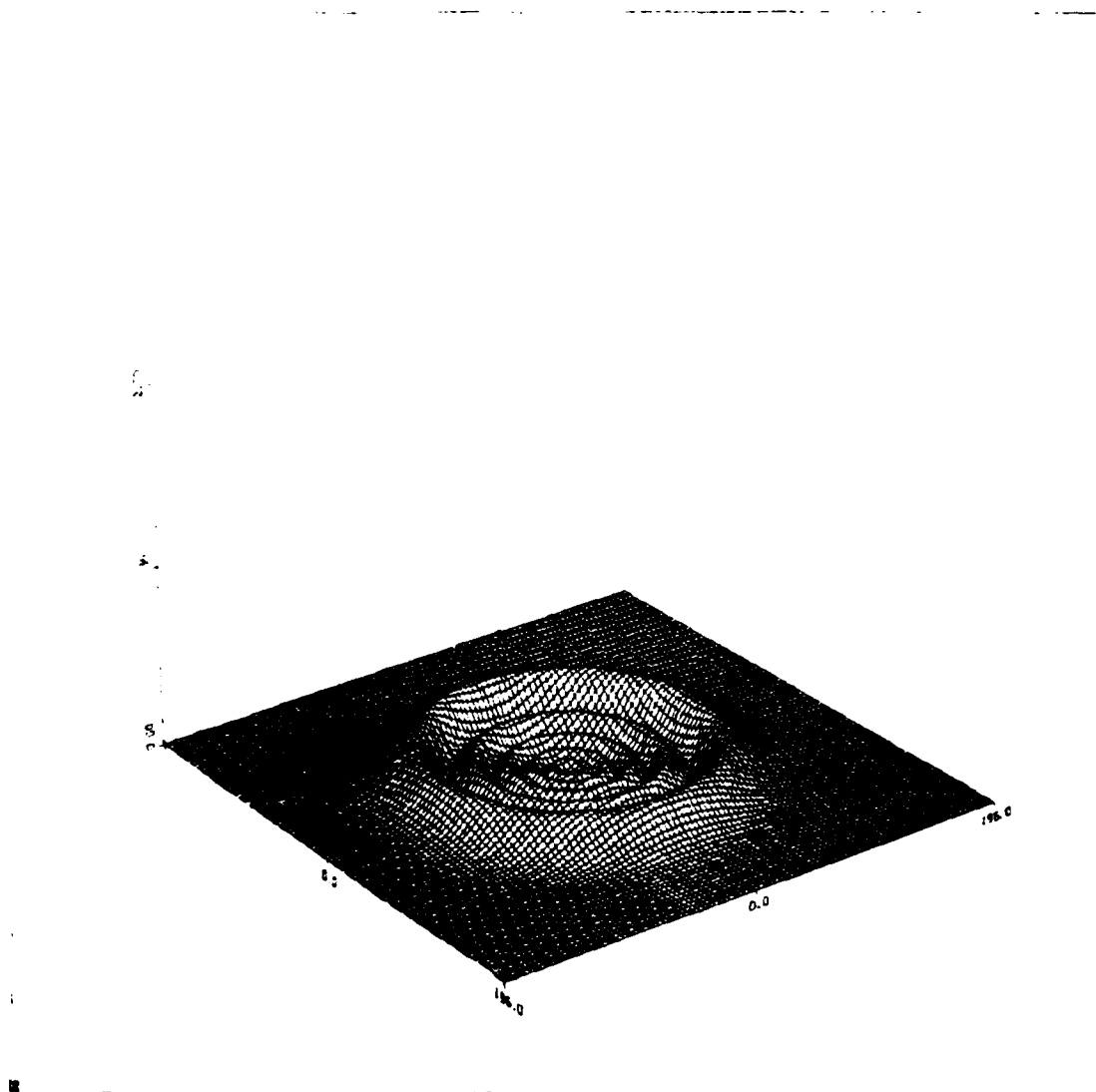


Fig. 9. Probability-Density for the Electron  $n = 8$ ,  $l = 3$

6.

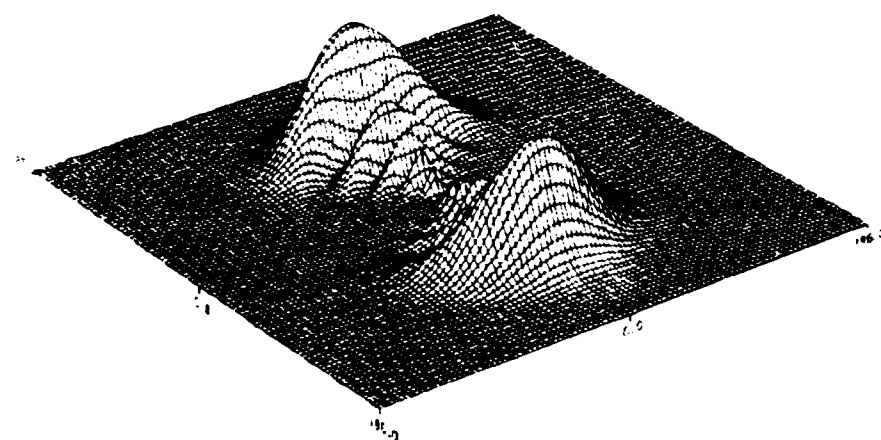


Fig. 10. Probability-Density for the Electron  $n = 8$ ,  $l = 3$ ,  $m = 3$

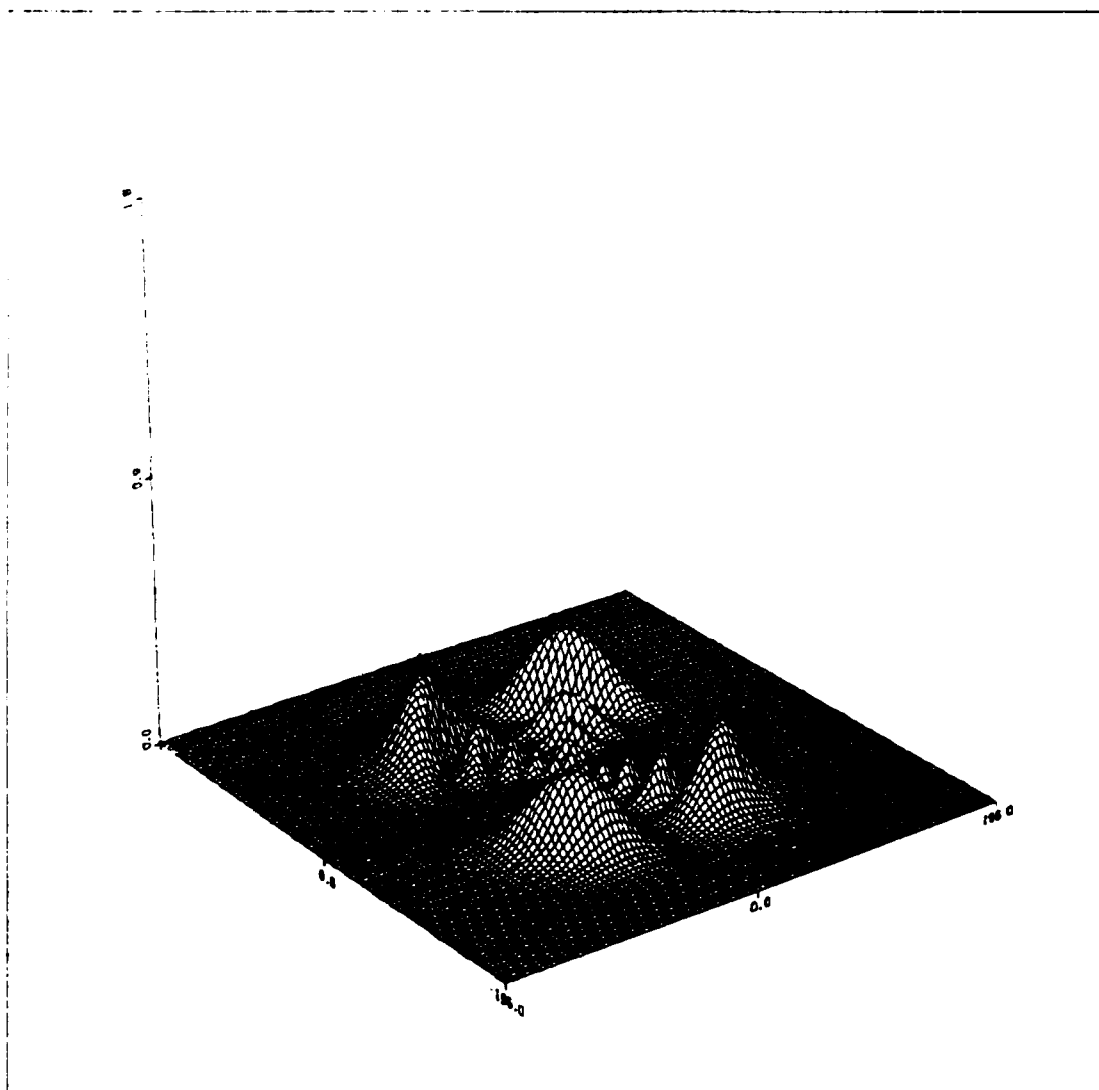


Fig. 11. Probability-Density for the Electron  $n = 8$ ,  $l = 3$ ,  $m = 2$

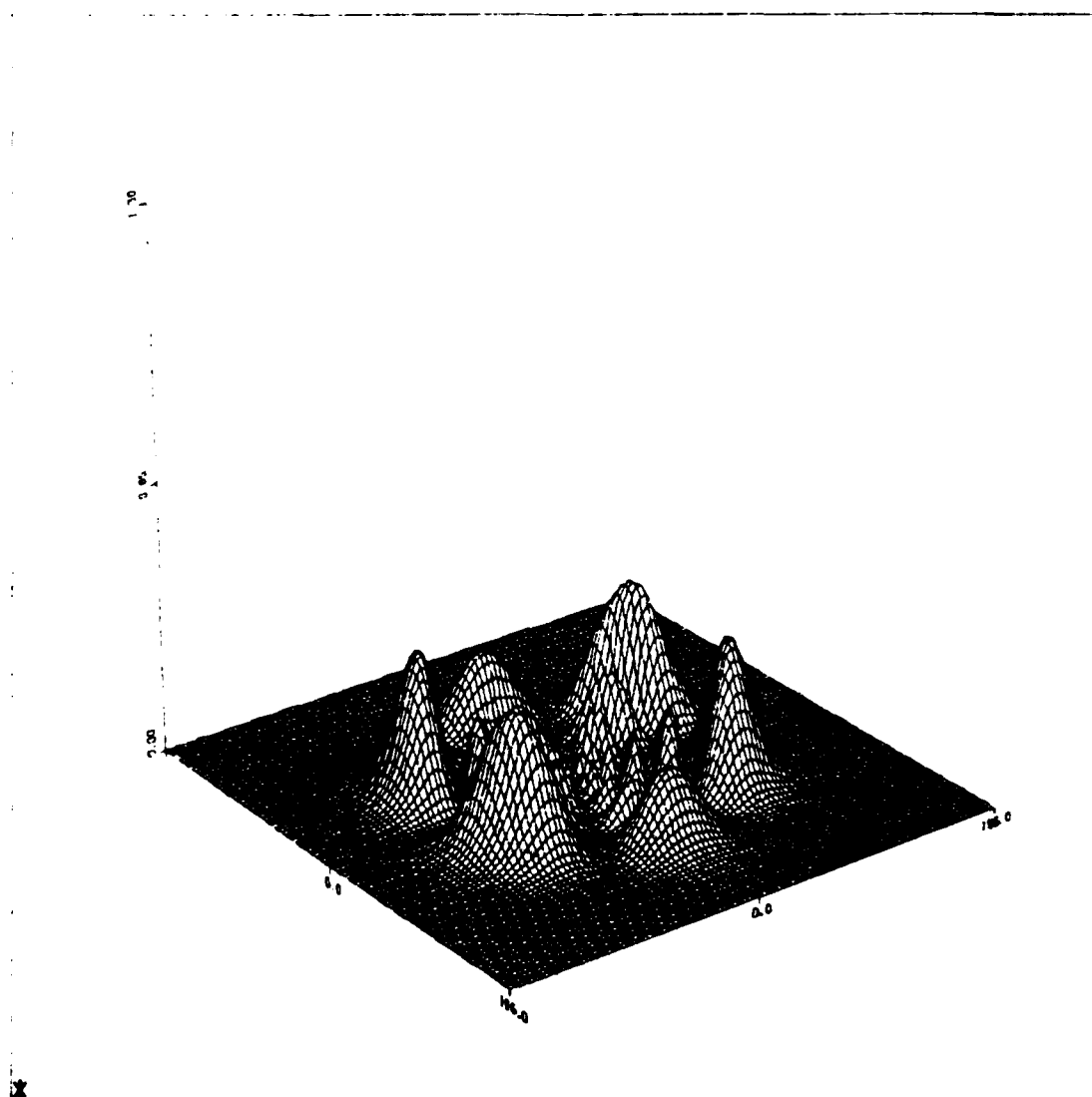


Fig. 12. Probability-Density for the Electron  $n = 8$ ,  $l = 3$ ,  $m = 1$

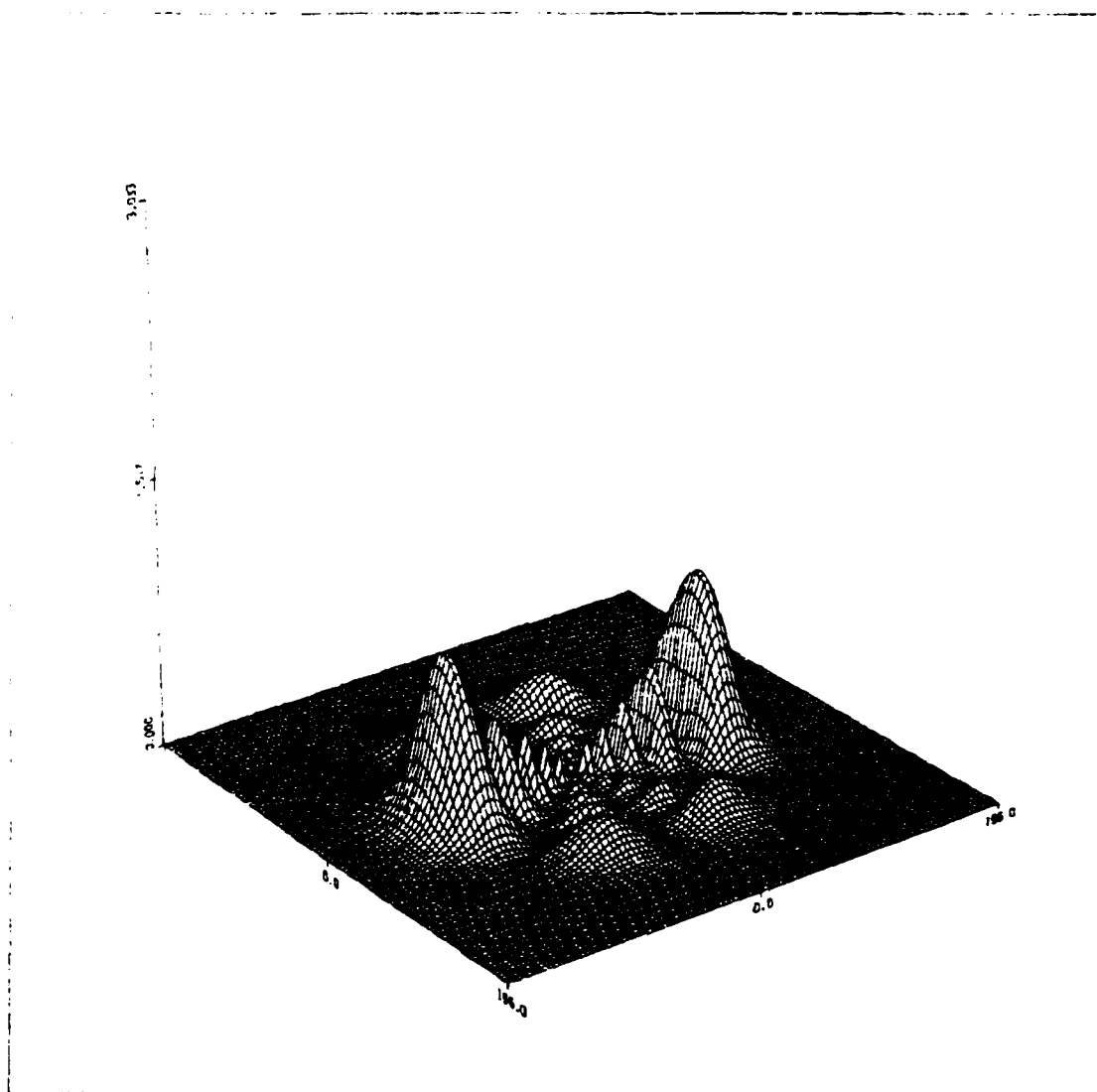


Fig. 13. Probability-Density for the Electron  $n = 8$ ,  $l = 3$ ,  $m = 0$

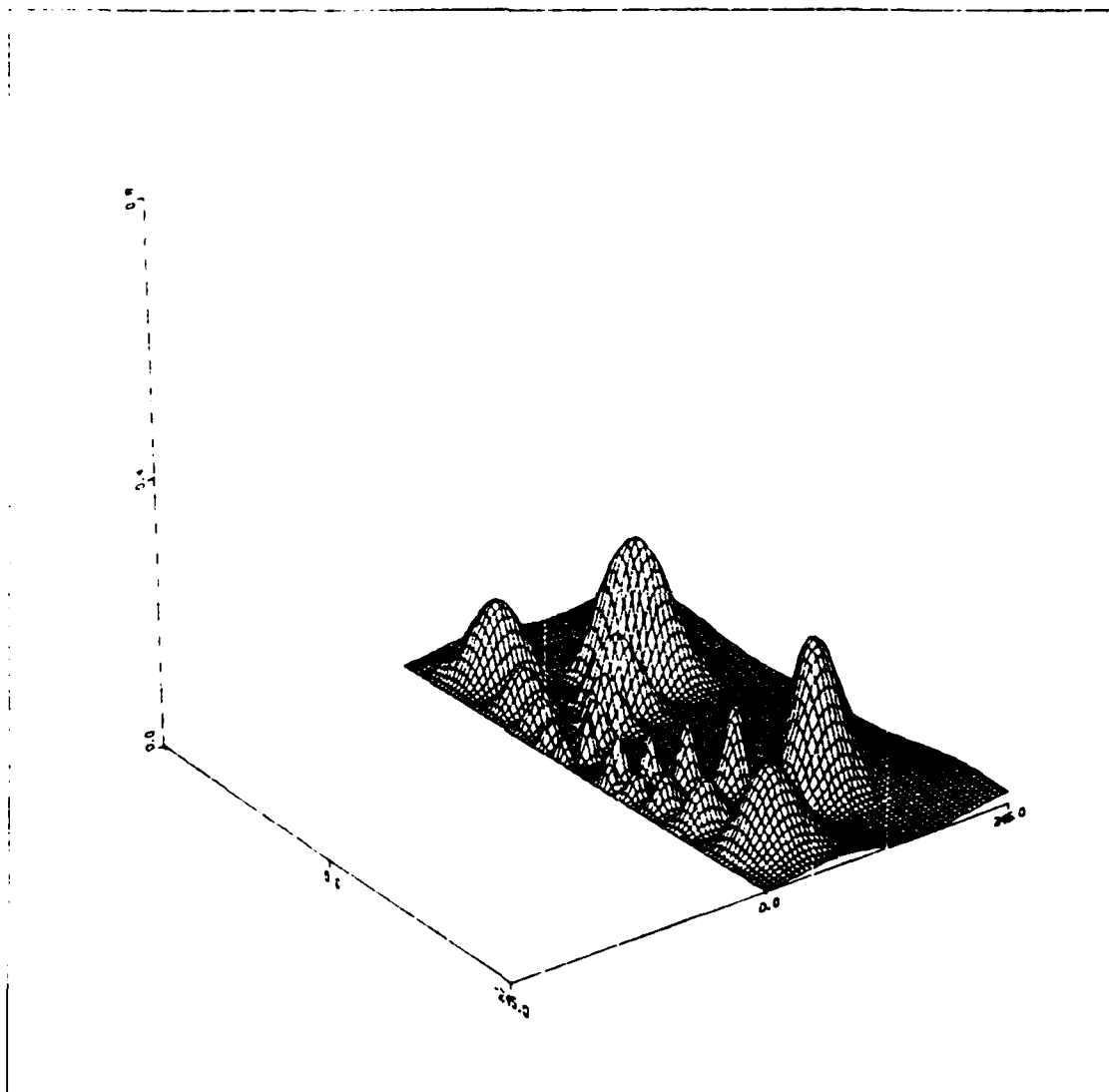


Fig. 14. Probability-Density for the Electron  $n = 11$ ,  $l = 6$ ,  $m = 3$   
(Half Plot)

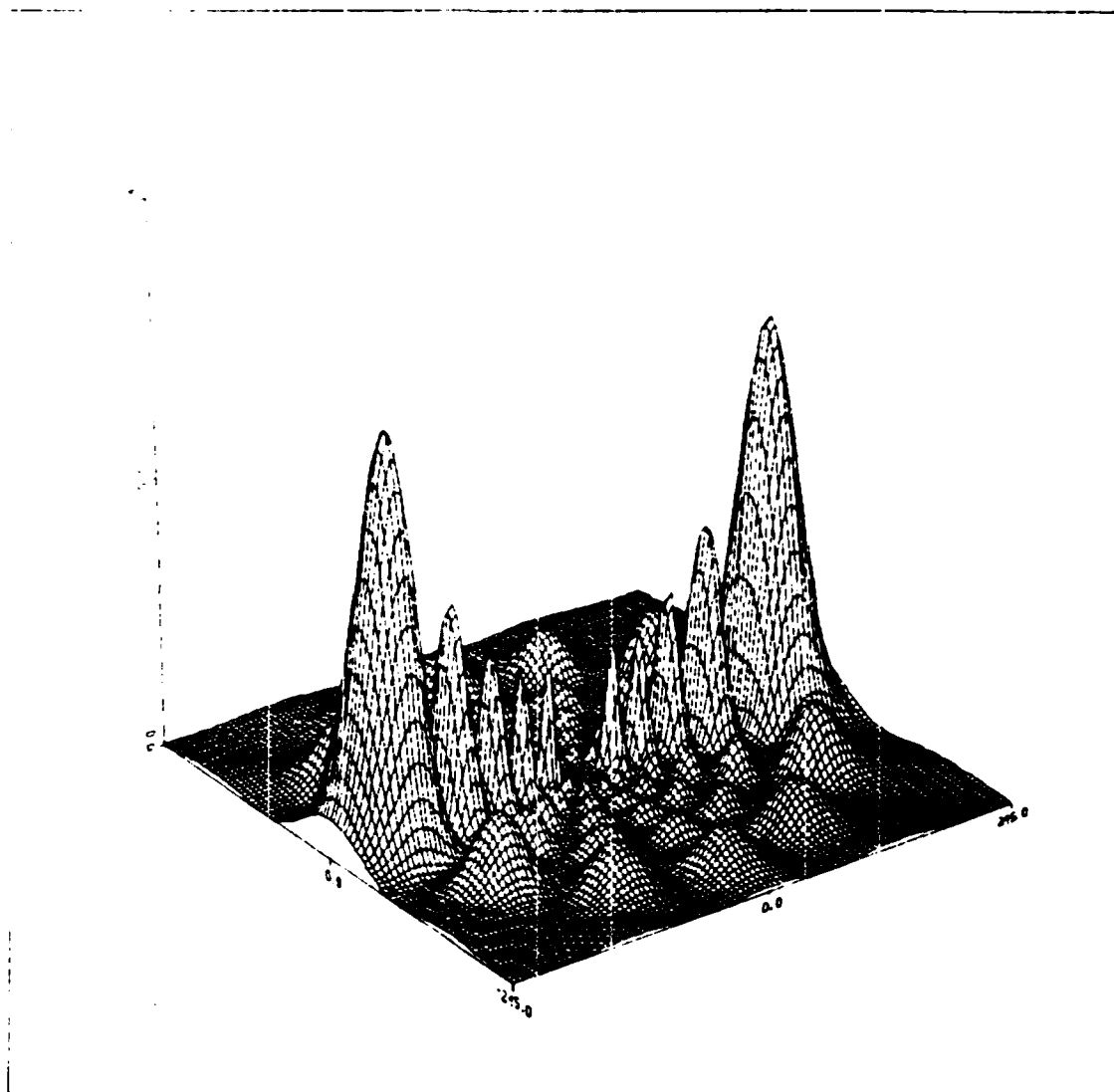


Fig. 15. Probability-Density for the Electron  $n = 11$ ,  $l = 6$ ,  $m = 0$

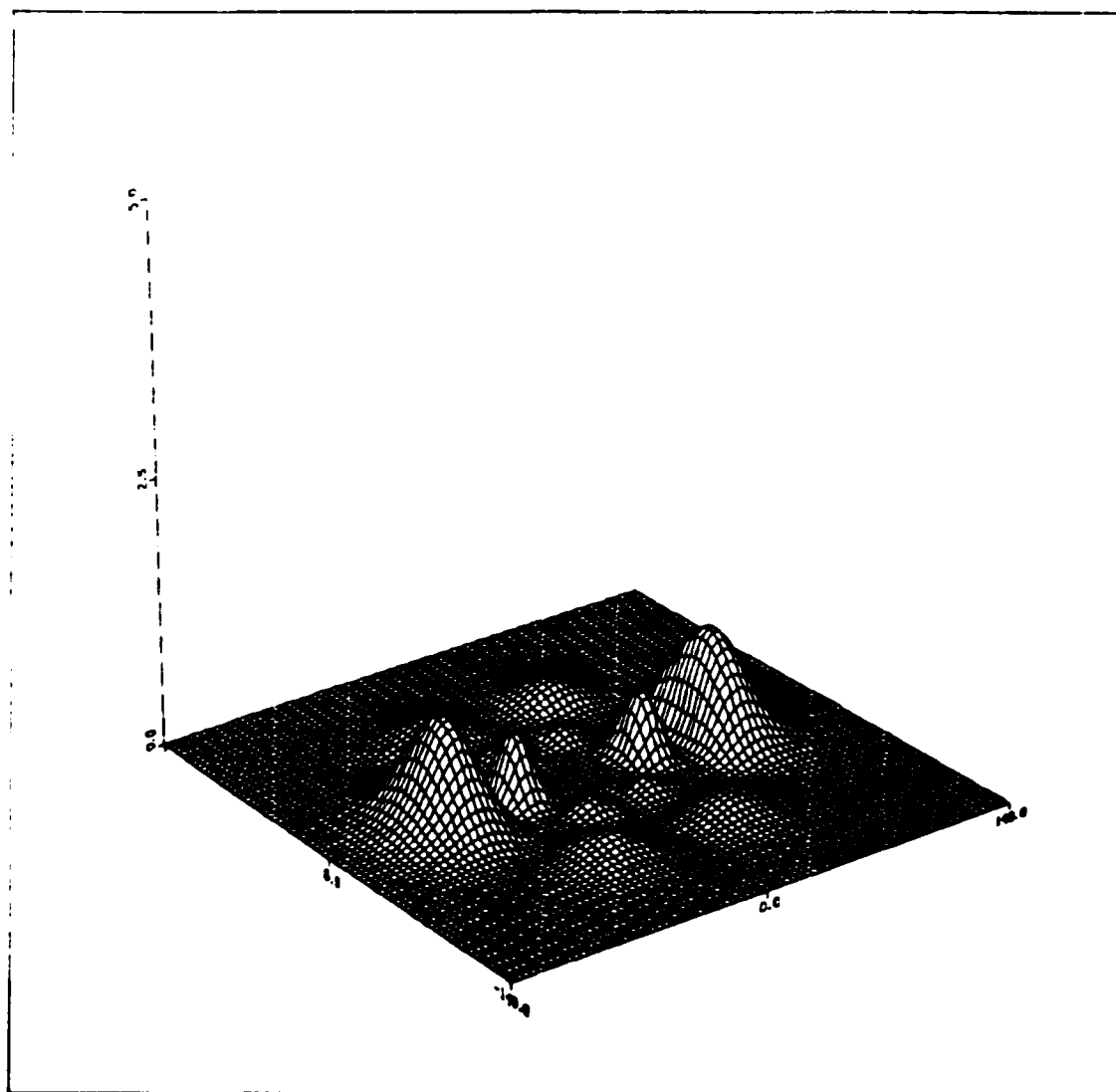


Fig. 16. Probability-Density for the Electron  $n = 8$ ,  $l = 6$ ,  $m = 0$

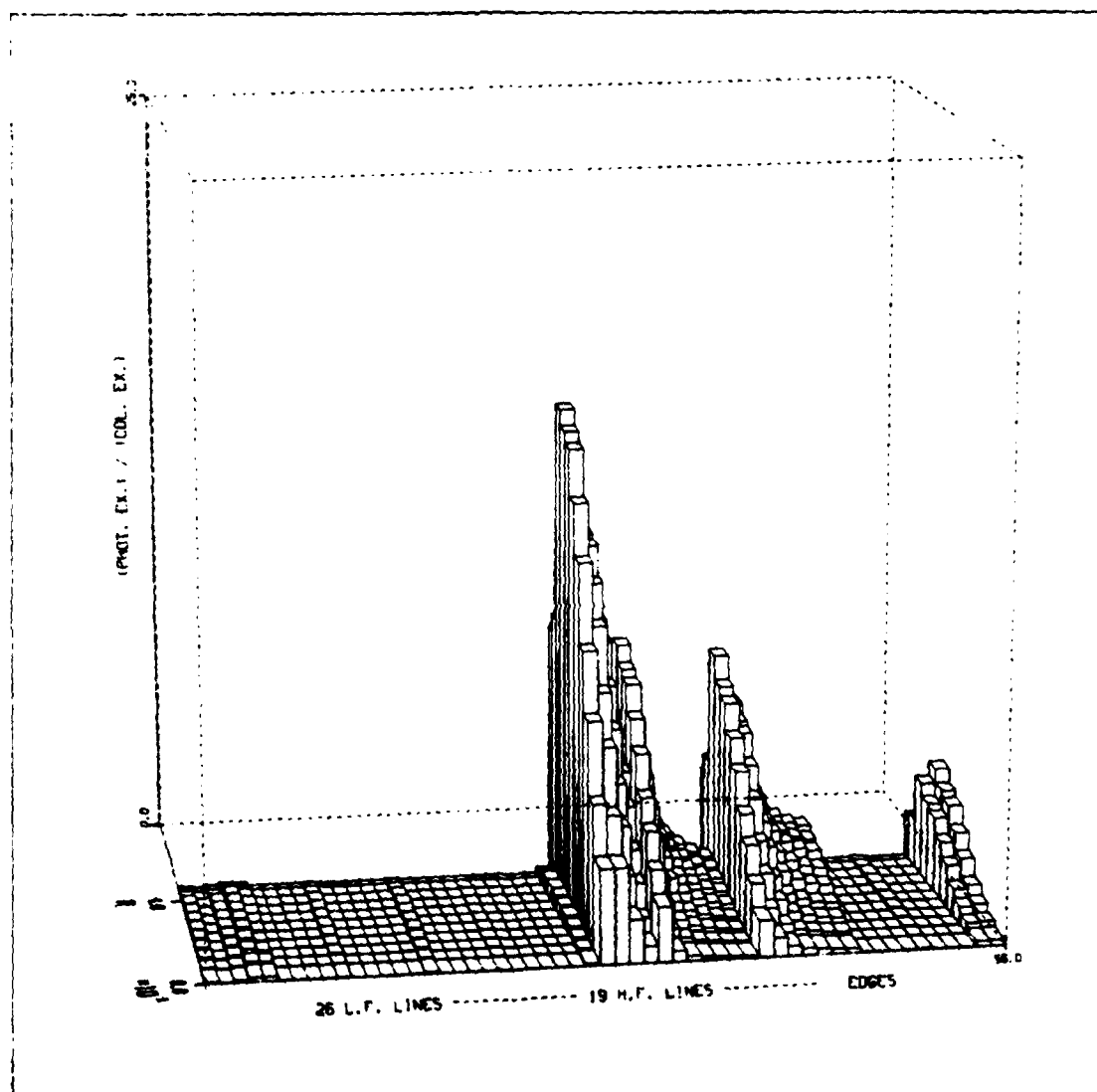


Fig. 17. (Photo Excitation/Collisional Excitation) at  $t = 7.5 \times 10^{-10}$  sec. for 55 Lines and Edges

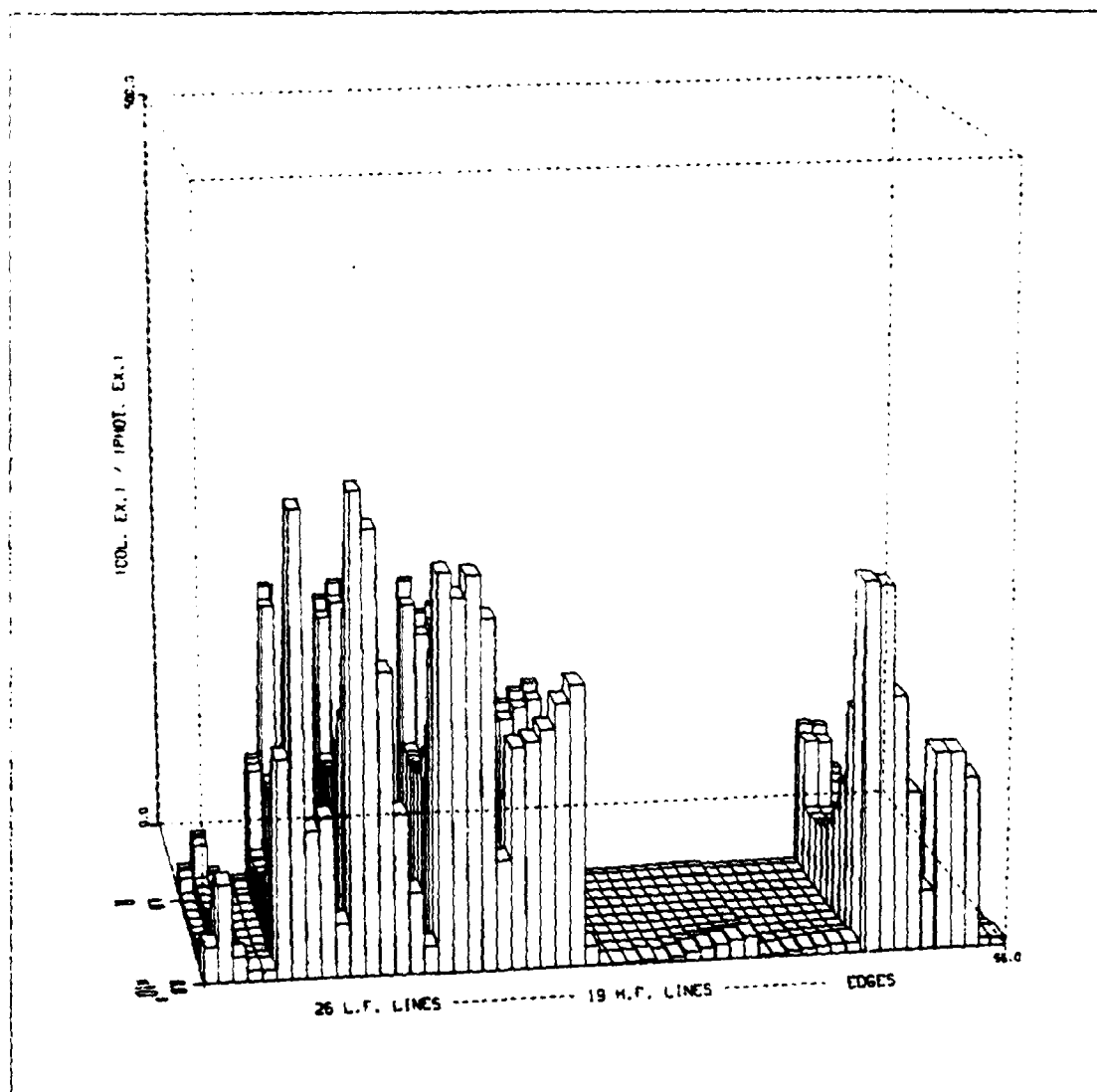


Fig. 18. (Collisional Excitation/Photo Excitation) at  $t = 7.5 \times 10^{-10}$  sec. for 55 Lines and Edges

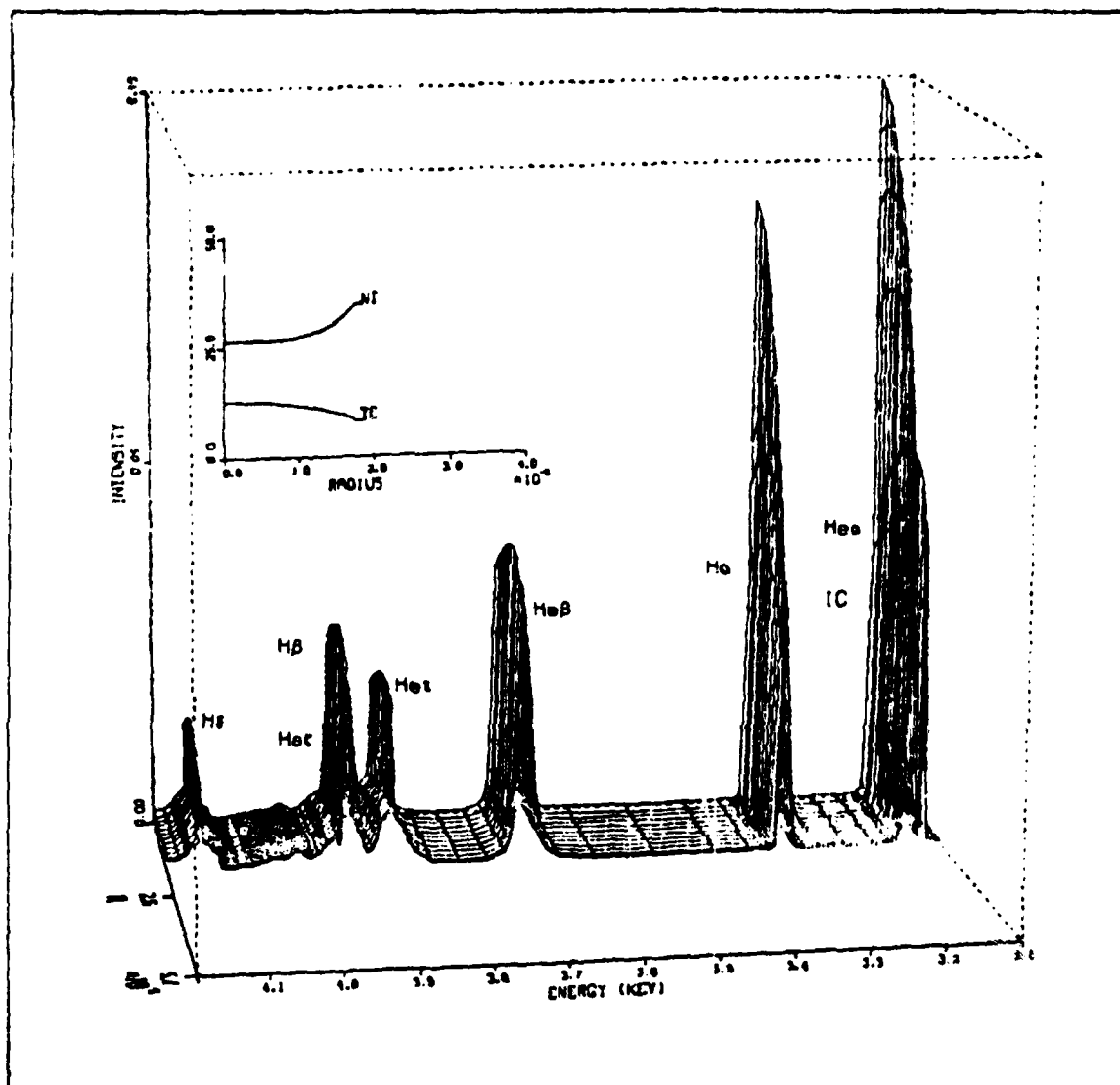


Fig. 19. Black and White Copy from the Color Movie of the NRL/LASNEX Case

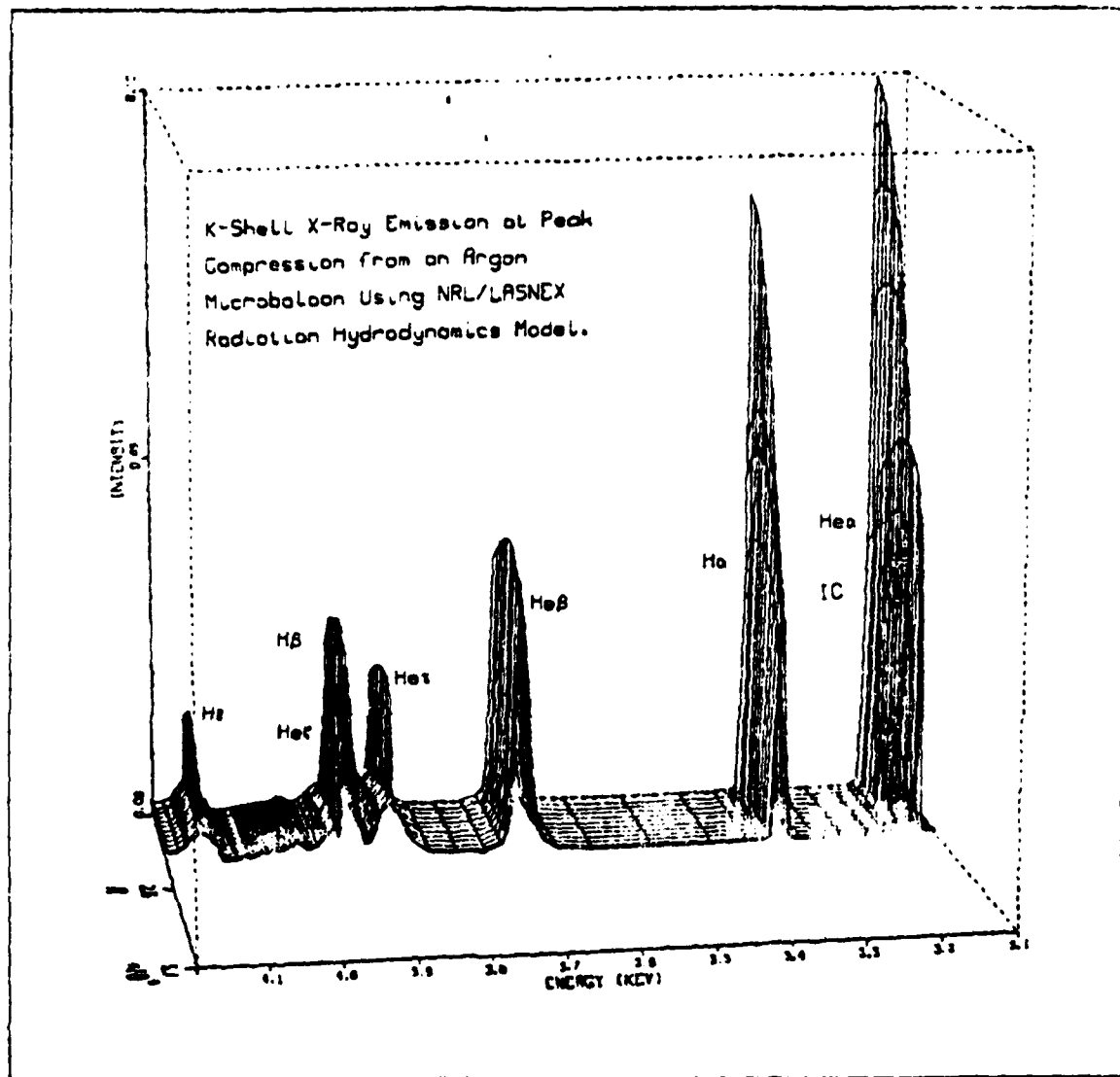


Fig. 20. Black and White Copy from the Color Set of Pictures of the NRL/LASNEX Case

DATE  
FILMED  
0-8